HHS Public Access

Author manuscript

Science. Author manuscript; available in PMC 2018 March 24.

Published in final edited form as:

Science. 2017 March 24; 355(6331): 1324–1330. doi:10.1126/science.aah6893.

PI3K pathway regulates ER-dependent transcription in breast cancer through the epigenetic regulator KMT2D

Eneda Toska[1], **Hatice U. Osmanbeyoglu**[2,*], **Pau Castel**[1,3,*], **Carmen Chan**[1], **Ronald C. Hendrickson**[4], **Moshe Elkabets**[1,5], **Maura N. Dickler**[6], **Maurizio Scaltriti**[1,7], **Christina S. Leslie**[2], **Scott A. Armstrong**[8,9], and **José Baselga**[1,6]

[1]Human Oncology and Pathogenesis Program, Memorial Sloan Kettering Cancer Center, 1275 York Avenue, Box 20, New York, NY 10065, USA

[2]Computational Biology Program, Memorial Sloan Kettering Cancer Center, 1275 York Avenue, Box 460, New York, NY 10065, USA

[3]Helen Diller Family Comprehensive Cancer Center, University of California–San Francisco, 1450 3rd Street, San Francisco, CA 94158, USA

[4]Microchemistry and Proteomics Core Laboratory, Memorial Sloan Kettering Cancer Center, New York, NY 10065, USA

[5]The Shraga Segal Department of Microbiology, Immunology and Genetics, Faculty of Health Sciences, Ben-Gurion University of the Negev, Beer-Sheva 84105, Israel

[6]Department of Medicine, Memorial Sloan Kettering Cancer Center, New York, NY 10065, USA

[7]Department of Pathology, Memorial Sloan Kettering Cancer Center, New York, NY 10065, USA

[8]Cancer Biology and Genetics Program, Memorial Sloan Kettering Cancer Center, New York, NY 10065, USA

[9]Department of Pediatric Oncology, Dana-Farber Cancer Institute, 450 Brookline Avenue, Boston, MA 02215, USA

Abstract

Activating mutations in *PIK3CA*, the gene encoding phosphoinositide-(3)-kinase α (PI3Kα), are frequently found in estrogen receptor (ER)–positive breast cancer. PI3Kα inhibitors, now in late-stage clinical development, elicit a robust compensatory increase in ER-dependent transcription that limits therapeutic efficacy. We investigated the chromatin-based mechanisms leading to the activation of ER upon PI3Kα inhibition. We found that PI3Kα inhibition mediates an open chromatin state at the ER target loci in breast cancer models and clinical samples. KMT2D, a histone H3 lysine 4 methyltransferase, is required for FOXA1, PBX1, and ER recruitment and activation. AKT binds and phosphorylates KMT2D, attenuating methyltransferase activity and ER function, whereas PI3Kα inhibition enhances KMT2D activity. These findings uncover a

Correspondence to: Scott A. Armstrong; José Baselga.

*These authors contributed equally to this work

Supplementary Materials: www.sciencemag.org/content/355/6331/1324/suppl/DC1 Materials and Methods Figs. S1 to S8 Tables S1 to S3 References (34–44)

mechanism that controls the activation of ER by the posttranslational modification of epigenetic regulators, providing a rationale for epigenetic therapy in ER-positive breast cancer.

Activating mutations in the *PIK3CA* gene occur at high frequency in estrogen receptor (ER)–positive breast cancer, indicating that the PI3K signaling pathway plays an important role in tumorigenesis (1, 2). Consistent with this, PI3Kα inhibitors have shown antitumor activity in patients with *PIK3CA*-mutant, ER-positive breast cancer (3, 4). However, a number of mechanisms of resistance have emerged that could potentially limit their efficacy (5, 6). We have observed an adaptive tumor response to PI3Kα inhibitors that is characterized by an increase in ER-dependent transcription, which mediates therapeutic resistance and can be reversed by the addition of anti-ER therapies (7). These findings have led to pilot clinical studies of combination therapies consisting of PI3Kα inhibitors and anti-ER agents that have produced high response rates and prolonged clinical benefit, even in tumors refractory to ER therapies (8–10). These findings have triggered the launch of two phase III registration clinical studies testing PI3Kα inhibitors in combination with the anti-ER agent fulvestrant (11, 12). The mechanisms by which tumor cells exposed to PI3Kα inhibitors activate ER signaling are not well understood. In luminal breast cancers, ER is a master regulator of transcription, activating expression of genes that favor tumor growth and survival (13). Binding of ER to estrogen-responsive elements (EREs) leads to recruitment of additional cooperating transcription factors (TFs) that are essential for the function of this intricate network (13–15).

To investigate the cis-regulatory elements and cofactors involved in ER-dependent transcription induced by treatment with a PI3Kα inhibitor (namely, BYL719) (16), we performed ER chromatin immunoprecipitation followed by high-throughput sequencing (ChIP-seq) in the breast cancer cell line T47D. PI3Kα inhibition induced differential ER binding, as demonstrated by gained or lost ER-binding events (Fig. 1A). As expected, the ERE motif was highly enriched in the gained ER-binding sites upon treatment with BYL719. The forkhead box A1 (FOXA1) motif and a homeobox class motif were also enriched, suggesting the presence of these TFs at the ER-binding sites. FOXA1 is required for ER-chromatin interactions (14). PBX1 (pre–B cell leukemia homeobox 1), a FOXA1 collaborator and a member of the homeobox family that is required for optimal ER activity (15), was most likely associated with the homeobox class motif found in our analysis (Fig. 1A and fig. S1A).

FOXA1 ChIP-seq analysis in T47D cells revealed a differential binding profile of FOXA1 upon PI3Kα inhibition. A nuclear receptor and a homeobox class motif, suggestive of ER and PBX1, respectively, were among the most enriched motifs within the enhanced FOXA1-binding regions (Fig. 1B and fig. S1B). An increased co-occupancy of ER and FOXA1 was also observed upon BYL719 treatment at specific target loci (Fig. 1C and fig. S1C). Hence, we hypothesized that (i) PI3Kα inhibition enhances the binding of the FOXA1-PBX1-ER regulatory network to chromatin and (ii) FOXA1 or PBX1 may be involved in ER activation in this setting. To assess the role of FOXA1 and PBX1 in the activation of ER at the chromatin level, we performed ChIP-quantitative polymerase chain reaction (qPCR) in T47D and MCF7 breast cancer cells to examine the binding of these TFs to the enhancers or

promoters of canonical ER target genes. The binding of ER, FOXA1, and PBX1 was substantially enhanced upon PI3Kα inhibition (fig. S1, D and E). FOXA1 and PBX1 were required for ER function in the context of PI3Kα therapeutic inhibition, as evidenced by the loss of ER binding and activity upon FOXA1 or PBX1 knockdown (Fig. 1, D and E, and figs. S2 and S3). We also conducted gene set enrichment analysis using our previously published transcriptomic data set (7) in T47D cells, MCF7 cells, and MCF7 xenografts to study the enrichment of nuclear receptors, FOXA1, and PBX1 upon PI3Kα inhibition. As expected, we observed strong enrichment of ER, FOXA1, and PBX1 in response to PI3Kα blockage (tables S1 to S3). PI3Kα inhibition also resulted in enrichment for several other nuclear receptors, such as PR (progesterone receptor), GR (glucocorticoid receptor), AR (androgen receptor), VDR (vitamin D receptor), and RAR (retinoic acid receptor), but at lower levels compared with those for ER (tables S1 to S3). These results suggest that ER is the nuclear receptor affected the most by PI3Kα inhibition in breast cancer.

We next explored the role of FOXA1 and PBX1 in enhancing ER function in response to PI3Kα inhibitors. FOXA1 or PBX1 silencing by either constitutive or inducible short hairpin RNAs (shRNAs) was sufficient to decrease the viability of cells treated with BYL719 (fig. S4, A to F). To investigate the in vivo activity of BYL719, we engineered MCF7 human breast cancer cells to express inducible shRNA against FOXA1 and then injected the cells into mice. Although FOXA1 silencing alone had no discernible effects on the growth of tumor xenografts, it markedly increased the antitumor activity of BYL719 (Fig. 1, F and G). Similar results were observed when PBX1 was knocked down in MCF7 xenografts (fig. S4, G and H). In these tumors, we also confirmed the reduction of ER occupancy when either FOXA1 or PBX1 was silenced (Fig. 1H and fig. S4I). Thus, FOXA1 or PBX1 silencing sensitizes cells to PI3Kα inhibition through suppression of ER activity.

To study the impact of PI3Kα inhibition on the global chromatin structure of the breast cancer epigenome, we used ATAC-seq (assay for transposase-accessible chromatin with sequencing), which enables the study of chromatin openness and the interplay between TFs and accessible chromatin regions. Genome-wide ATAC-seq in T47D cells revealed that PI3Kα inhibition induces substantial changes in chromatin state, as demonstrated by an increase in the gained and lost accessible chromatin sites (Fig. 2A). Analysis of the open chromatin patterns (Fig. 2B), a feature of active transcription, revealed responsive elements enriched for ER, FOXA1, and PBX1 (Fig. 2C), consistent with our previous findings. ATAC-seq signals peaked at regions where we had detected ER- and FOXA1-binding events by ChIP-seq—namely, ER canonical target genes (fig. S5, A and B).

Taking advantage of the feasibility of performing ATAC-seq with a limited number of cells (17), we next explored the epigenetic landscape of breast tumor samples from patients who had participated in a clinical trial with the PI3Kα inhibitor BYL719 (4). We studied the chromatin accessibility of two paired tumor biopsies that had been obtained before BYL719 therapy and while the patients were on therapy. We found that drug treatment induced an increase in chromatin accessibility in the regions previously identified to be responsive to PI3Kα inhibition (Fig. 2D and fig. S5C). Notably, the ATAC-seq signals detected in the patient samples peaked at the same genomic regions that had shown enhanced binding of ER and FOXA1 and enhanced chromatin accessibility in our cell line model. Moreover, similar

to our in vitro data, responsive elements for ER, FOXA1, and PBX1 were present in the open chromatin regions after in silico motif analysis, highlighting the specificity of our assay in the patient samples (Fig. 2E). We also performed RNA sequencing on 15 pre-and on-treatment tumor biopsies and found a substantial enrichment of ER-associated signatures induced by BYL719 treatment (fig. S5, D and E). Together, these data indicate that PI3Kα inhibition results in remodeling of the chromatin landscape to enhance ER-dependent transcription in breast cancer cell lines and patient tumor samples.

We next aimed to identify the epigenetic regulators that orchestrate the chromatin remodeling induced by PI3Kα inhibition. It has been previously shown that active histone modifications—mono- and dimethylated histone H3 lysine 4 (H3K4me1/2)—are associated with FOXA1 and PBX1 binding at their cis-regulatory elements (15, 18, 19). Additionally, KMT2D (also known as MLL2 or MLL4), a member of the COMPASS (complex of proteins associated with Set1)–like family, is a major H3K4me1/2 methyltransferase that facilitates gene expression (20–22) and has the ability to interact with ER through LXXLL motifs (L, leucine; X, any amino acid) (23). To explore whether KMT2D participates in the activation of the ER regulatory network after PI3Kα inhibition, we knocked down KMT2D and examined the recruitment of ER, FOXA1, and PBX1 and the expression of ER target genes. KMT2D knockdown in T47D and MCF7 cells resulted in a marked loss of binding of these TFs at ER-FOXA1-PBX1 shared target genes and a decrease in ER target gene expression upon BYL719 treatment (Fig. 3, A and B, and fig. S6, A and B). KMT2D suppression also led to a considerable decrease in H3K4me1/2 occupancy at representative ER canonical genes, consistent with the hypothesis that KMT2D catalyzes these histone modifications in breast cancer cells (fig. S6C). Although overexpression of wild-type KMT2D in cells depleted of endogenous KMT2D could restore the binding of these TFs, overexpression of KMT2D mutants deficient in methyltransferase activity (24) failed to do so (fig. S6D). Similarly, overexpression of the H3K4me1/2 demethylase KDM1 (25), which antagonizes KMT2D enzymatic action, abrogated the occupancy of ER, FOXA1, and PBX1 and the expression of ER-dependent genes upon PI3Kα inhibition (fig. S6, E to G). Collectively, these findings suggest that KMT2D is required for the activation of ER-dependent transcription upon PI3Kα inhibition and that it does this by catalyzing H3K4me1/2 modifications that support FOXA1, PBX1, and ER recruitment to specific chromatin sites.

Given our observation that KMT2D silencing suppresses ER activation, we hypothesized that loss of function of KMT2D might augment the therapeutic activity of BYL719 in ER-positive cells. Indeed, we found that KMT2D knockdown decreased cell viability in ER-positive T47D and MCF7 cell lines and had a greater effect when combined with BYL719 (fig. S7, A to C). In mice bearing MCF7 xenografts with doxycycline-inducible shRNA against KMT2D, silencing KMT2D resulted in a marked antitumor effect that was enhanced in the presence of BYL719 (Fig. 3, C and D). By performing ChIP-qPCR experiments in the in vivo tumor samples, we confirmed that binding of ER, FOXA1, and PBX1 was lost when KMT2D was knocked down (Fig. 3E). These findings suggest that targeting KMT2D in ER-positive breast cancers could be a potential therapeutic strategy to enhance the sensitivity of PI3Kα inhibitors.

Our finding that KMT2D is a critical determinant of ER function upon PI3Kα targeting prompted us to study how PI3K inhibition affects the binding dynamics of KMT2D at the chromatin level. We found that KMT2D recruitment at gene regulatory regions peaked early in BYL719 treatment at ER target genes but not at control genes—namely, ER-FOXA1-PBX1 targets whose expression did not change upon BYL719 treatment (Fig. 3F and fig. S7, D and E). The abundance of H3K4me1/2 occupying these regions was also elevated at the same time points, as were total H3K4 methyltransferase activity and H3K4me1/2 protein levels (Fig. 3, F to H, and fig. S7D). In addition, KMT2D ChIP-seq assay in T47D cells revealed that KMT2D binding peaked at several regions that showed differential binding of ER and FOXA1 upon treatment with the PI3Kα inhibitor (fig. S7F). The tight temporal correlation between PI3Kα inhibition and changes in KMT2D recruitment, H3K4 methyltransferase activity, and abundance of H3K4me1/2 suggests a direct regulation of KMT2D activity by the PI3K pathway.

Oncogenic PI3K signaling regulates several downstream effectors through kinases that can phosphorylate these effectors. Among these kinases, the serine/threonine (S/T) kinase AKT phosphorylates a large number of substrates by recognizing the consensus motif RXRXX(S/T) (R, arginine) (26). We observed that the KMT2D protein sequence contains two RXRXX(S/T) consensus sites that are evolutionarily conserved (Fig. 4A). Although the consensus site at S1762 could not be detected by mass spectrometry because of the surrounding lysine-rich region, which renders it sensitive to trypsin digestion, we found that S1331 was phosphorylated (fig. S8, A and B). We therefore focused on the S1331 site for the remaining experiments. Coimmunoprecipitation assay using ectopically expressed HA (hemagglutinin epitope)–tagged KMT2D and V5-tagged AKT1 in 293T cells revealed that KMT2D physically interacts with AKT1. We further confirmed the interaction between endogenous KMT2D and AKT by coimmunoprecipitation in T47D cells (Fig. 4, B and C). We next identified the region of KMT2D that interacts with AKT1. Given the large size of KMT2D (~593 kDa), we performed coimmunoprecipitation assays using five non-overlapping fragments of KMT2D (Fig. 4D) and found that AKT1 binds the 1222–1819 amino acid region of KMT2D, where the S1331 phosphorylation site resides (Fig. 4E). In vitro kinase assays confirmed the ability of AKT to directly phosphorylate S1331, as detected by the phospho-RXRXX(S/T) and phospho-KMT2D (S1331) antibodies (Fig. 4F and fig. S8C). Endogenous KMT2D was found to be more phosphorylated at S1331 in isogenic MCF10A cells that harbor the activating H1047R mutation of *PIK*3*CA,* commonly found in breast cancer, as compared with those harboring wild-type *PIK3CA* (fig. S8D). Treatment of ER-positive cell lines with either PI3K or AKT inhibitors reduced S1331 phosphorylation (fig. S8, E and F). Next, we sought to determine how phosphorylation of KMT2D by AKT affects KMT2D activity. Mutation of KMT2D S1331 to the nonphosphorylatable amino acid alanine (S1331A) increased H3K4 methyltransferase activity and the levels of H3K4me1/2. Conversely, mutation of this site to the phosphomimetic amino acid aspartic acid (S1331D) decreased the levels of KMT2D activity (Fig. 4, G and H), suggesting that this phosphorylation event suppresses KMT2D methyltransferase activity, leading to a decrease in ER function. Consistent with this hypothesis, we observed an increase in ER, FOXA1, PBX1, and H3K4me1/2 binding at ER loci in S1331A KMT2D–expressing cells (Fig. 4I and fig. S8G).

Our data support a key role for KMT2D in modulating the chromatin competence necessary for the assembly of the ER-FOXA1-PBX1 transcriptional regulatory network. The net effect on ER transcriptional output leads to a diminution in the therapeutic efficacy of PI3K inhibitors. Direct phosphorylation of KMT2D by AKT suppresses the methyltransferase activity of KMT2D, which in turn suppresses ER transcriptional activity (fig. S8H). Conversely, inhibition of the PI3K-AKT pathway increases KMT2D activity, which facilitates the recruitment of a FOXA1-PBX1-ER regulatory network, unleashing a robust ER-dependent transcriptional program.

We speculate that phosphorylated KMT2D may function as a biomarker of resistance to therapeutic agents targeting PI3K and AKT in hormone-dependent malignancies. Our findings delineate the epigenetic mechanisms associated with ER activation by the PI3K pathway and directly connect an oncogenic signaling pathway with chromatin-based control of gene expression. The possibility that PI3K-AKT signaling alters the transcriptional repertoires of cancer cells by modulating the function of additional histone methyltransferases remains to be investigated. In agreement with studies in which epigenetic regulators such as EZH2 (27–29), KDM5A (30), DOT1L (31), LSD1 (32), MLL3 (33), and others have been shown to be critical in oncogenesis, our findings highlight the importance of epigenetic regulators in cancer and their potential as therapeutic targets. The discovery of the specific role of KMT2D in the interplay between ER and PI3K signaling provides a rationale for epigenetically informed combination therapies with PI3K inhibitors in ER-positive breast cancer.

Supplementary Material

Refer to Web version on PubMed Central for supplementary material.

Acknowledgments

We are grateful to L. Pasqualucci, who provided the pCMV-HA-KMT2D and the corresponding mutants, the N5437S and R5432W KMT2D plasmids. We also thank A. Shilatifard, who provided the KMT2D antibody for our preliminary experiments; P. Giresi, A. Krivtsov, and Y. Li for help with ATAC-seq; Y. Zou for help with ChIP-seq; N. Morse for help with xenograft establishment; and N. Socci for help with microarray analysis. This work was supported by NIH grant RO1CA190642-01A1, the Breast Cancer Research Foundation, and the Geoffrey Beene Cancer Research Center (to J.B.); National Cancer Institute (NCI) Cancer Center Support Grant P30CA08748 to the Microchemistry and Proteomics Core Laboratory of the Memorial Sloan Kettering Cancer Center; and NIH grants CA66996 and CA140575 to S.A.A. We are also grateful for the support of T. and B. Weinstein. E.T. holds a fellowship from the Terri Brodeur Breast Cancer Foundation. H.U.O. is supported by NCI award K99 CA207871. J.B. and M.N.D. are paid consultants for Novartis Pharmaceuticals. S.A.A. is a paid consultant for Epizyme, Imago Biosciences, and Vitae Pharmaceuticals. Memorial Sloan Kettering Cancer Center and the authors (E.T., S.A.A., and J.B.) have filed a patent application (U.S. patent registration number 62/420324) related to KMT2D inhibition as a treatment for breast cancer. The sequencing data have been deposited in the Gene Expression Omnibus database under accession numbers GEO GSE84515, GSE84593, GSE84594, and GSE95366.

References and Notes

1. Cancer Genome Atlas Network. Nature. 2012; 490:61–70. [PubMed: 23000897]
2. Ciriello G, et al. Cell. 2015; 163:506–519. [PubMed: 26451490]
3. Juric D, et al. Cancer Res. 2013; 73:LB–64.
4. Shah PD, et al. Cancer Res. 2015; 75:CT330.
5. Costa C, et al. Cancer Cell. 2015; 27:97–108. [PubMed: 25544637]

6. Juric D, et al. Nature. 2015; 518:240–244. [PubMed: 25409150]
7. Bosch A, et al. Sci Transl Med. 2015; 7:283ra51.
8. Janku F, et al. Cancer Res. 2015; 75:PD5–5.
9. Mayer IA, et al. Clin Cancer Res. 2016; 23:26–34. [PubMed: 27126994]
10. Juric D, et al. Cancer Res. 2013; 73:PD1–3.
11. Baselga J, et al. J Clin Oncol. 2016; 34:TPS617.
12. Andre F, et al. J Clin Oncol. 2016; 34:TPS618.
13. Green KA, Carroll JS. Nat Rev Cancer. 2007; 7:713–722. [PubMed: 17721435]
14. Hurtado A, Holmes KA, Ross-Innes CS, Schmidt D, Carroll JS. Nat Genet. 2011; 43:27–33. [PubMed: 21151129]
15. Magnani L, Ballantyne EB, Zhang X, Lupien M. PLOS Genet. 2011; 7:e1002368. [PubMed: 22125492]
16. Fritsch C, et al. Mol Cancer Ther. 2014; 13:1117–1129. [PubMed: 24608574]
17. Buenrostro JD, Giresi PG, Zaba LC, Chang HY, Greenleaf WJ. Nat Methods. 2013; 10:1213–1218. [PubMed: 24097267]
18. Eeckhoute J, et al. Genome Res. 2009; 19:372–380. [PubMed: 19129543]
19. Lupien M, et al. Cell. 2008; 132:958–970. [PubMed: 18358809]
20. Herz HM, et al. Genes Dev. 2012; 26:2604–2620. [PubMed: 23166019]
21. Hu D, et al. Mol Cell Biol. 2013; 33:4745–4754. [PubMed: 24081332]
22. Shilatifard A. Annu Rev Biochem. 2012; 81:65–95. [PubMed: 22663077]
23. Mo R, Rao SM, Zhu YJ. J Biol Chem. 2006; 281:15714–15720. [PubMed: 16603732]
24. Zhang J, et al. Nat Med. 2015; 21:1190–1198. [PubMed: 26366712]
25. Kooistra SM, Helin K. Nat Rev Mol Cell Biol. 2012; 13:297–311. [PubMed: 22473470]
26. Pearce LR, Komander D, Alessi DR. Nat Rev Mol Cell Biol. 2010; 11:9–22. [PubMed: 20027184]
27. Cha TL, et al. Science. 2005; 310:306–310. [PubMed: 16224021]
28. Kim W, et al. Nat Chem Biol. 2013; 9:643–650. [PubMed: 23974116]
29. McCabe MT, et al. Nature. 2012; 492:108–112. [PubMed: 23051747]
30. Spangle JM, et al. Cell Rep. 2016; 15:2692–2704. [PubMed: 27292631]
31. Nguyen AT, Taranova O, He J, Zhang Y. Blood. 2011; 117:6912–6922. [PubMed: 21521783]
32. Harris WJ, et al. Cancer Cell. 2012; 21:473–487. [PubMed: 22464800]
33. Jozwik KM, Chernukhin I, Serandour AA, Nagarajan S, Carroll JS. Cell Rep. 2016; 17:2715–2723. [PubMed: 27926873]

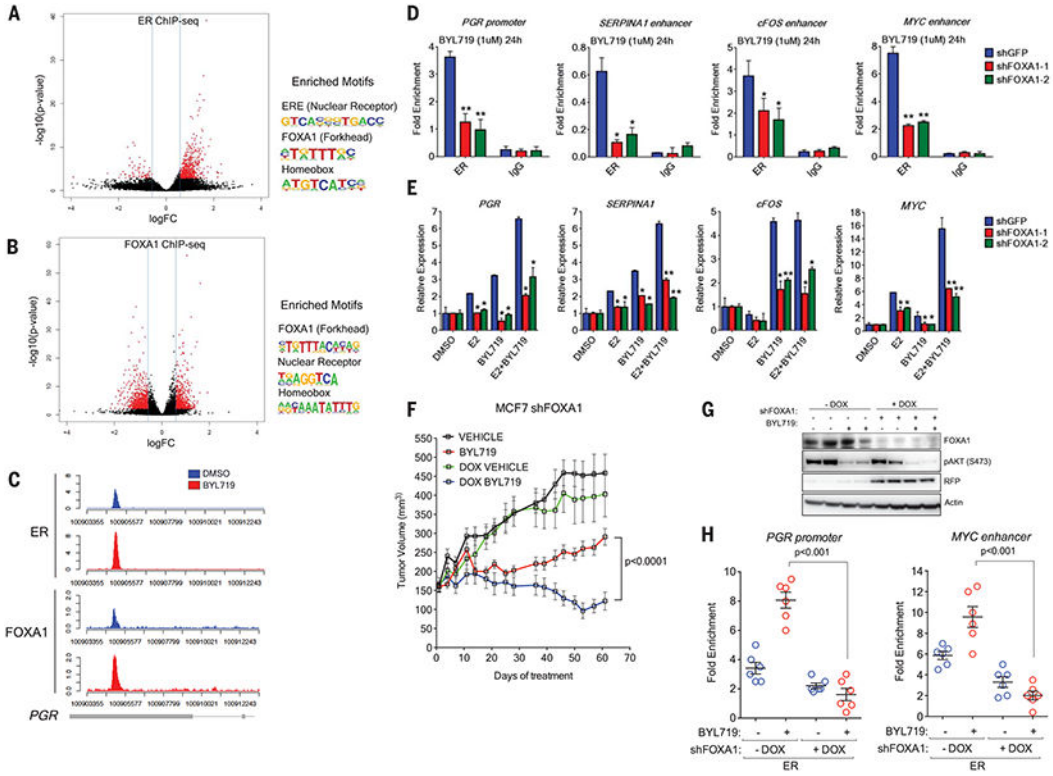

Fig. 1. FOXA1 and PBX1 are required for the activation of ER function upon PI3Kα inhibition

(**A** and **B**) Volcano plot of ER (**A**) and FOXA1 (**B**) ChIP-seq for T47D breast cancer cells treated with dimethyl sulfoxide (DMSO) or BYL719 (1 μM) for 24 hours. The *x* axis shows the log fold change (logFC), and they axis shows -$\log_{10}$(P value). The red dots correspond to the ER- or FOXA1-binding sites that are differentially bound upon BYL719 treatment compared with DMSO treatment. Also shown are the top enriched motifs observed at the gained ER- or FOXA1-binding events upon BYL719 treatment. At the gained ER-binding events: ERE, estrogen-responsive element ($P = 1 \times 10^{-70}$); FOXA1, forkhead ($P = 1 \times 10^{-27}$); and homeobox motif ($P = 1 \times 10^{-20}$). At the gained FOXA1-binding events: FOXA1 ($P = 1 \times 10^{-260}$), nuclear receptor class ($P = 1 \times 10^{-59}$), and homeobox motif ($P = 1 \times 10^{-29}$). (C) Example of a binding region of a BYL719-induced ER- and FOXA1-binding event (shown in reads per million). **(D)** ChIP-qPCR for ER occupancy in the enhancer and promoter regions after FOXA1 was knocked down by two distinct shRNAs in T47D cells upon treatment with BYL719 (1 μM) for 24 hours. IgG, immunoglobulin G. Values are shown as fold enrichment (i.e., the ratio of the mean percentage of input enrichment of the candidate gene to the mean percentage of input enrichment of a control gene). Error bars, SD ($n = 3$). *$P < 0.05$, **$P < 0.01$; Student's *t* test. **(E)** mRNA levels measured by reverse transcription (RT)-qPCR in T47D breast cancer cells maintained in estrogen-free media for 3 days, followed by treatment with DMSO, E2 (estrogen; 100 μm), BYL719 (1 μM), or E2 plus BYL719 for 24 hours. Error bars, SD ($n = 3$). *$P < 0.05$, **$P < 0.01$; Student's *t* test. **(F)** MCF7 shFOXA1 doxycycline (DOX)-inducible in vivo xenograft treated daily with vehicle or BYL719 (25 mg/kg) ($n = 10$ per group). The indicated P values were calculated using Student's *t* test. Error bars, ±SEM. **(G)** Western blot analysis of lysates of tumors collected at the end of the experiment, 4 hours after the last dose. **(H)** Tissue ChIP-qPCR assay for ER

occupancy in the candidate target genes of randomly collected tumors at the end of the experiment. *P* values were calculated using Student's *t* test. Error bars, ±SEM.

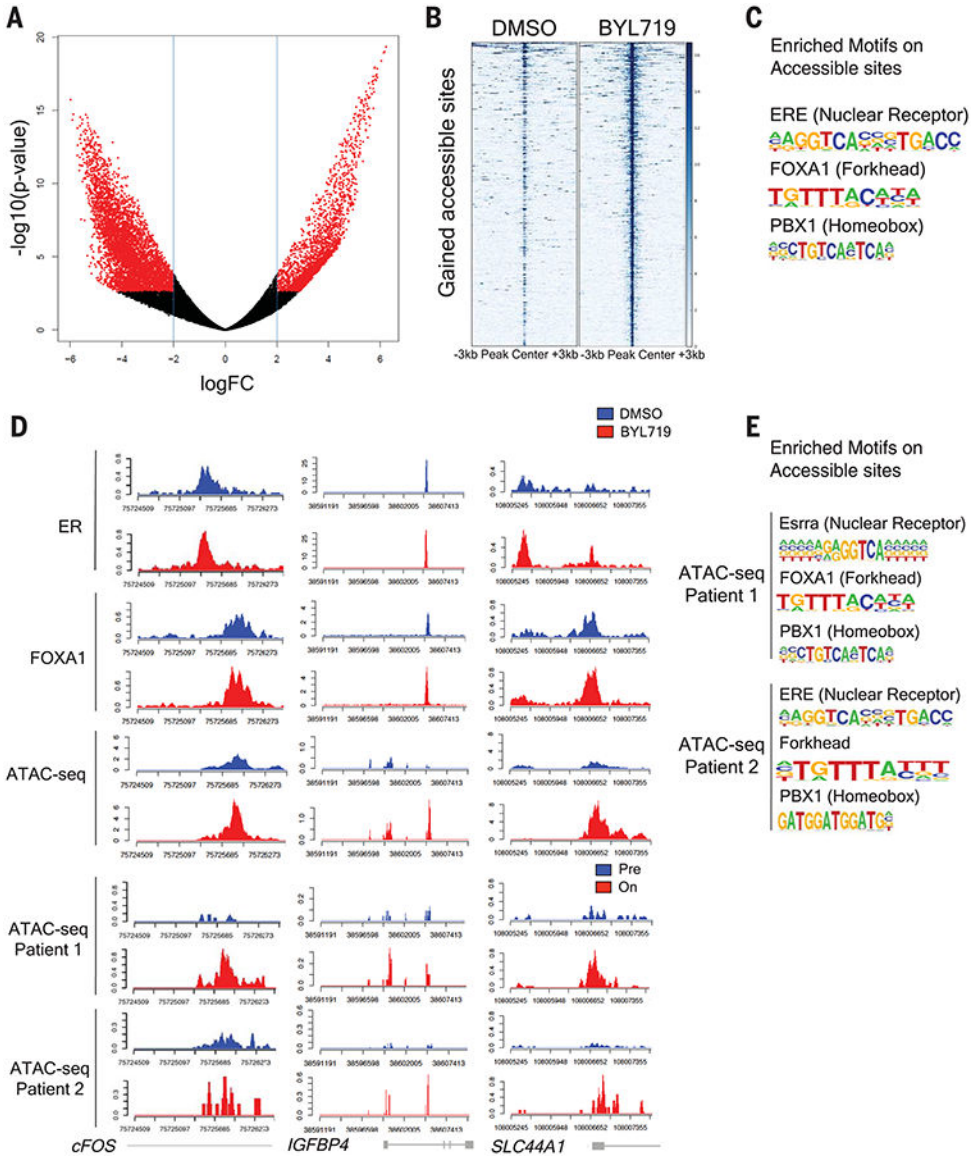

Fig. 2. PI3Kα inhibition remodels the chromatin landscape, leading to activation of ER-dependent transcription

(**A**) Volcano plot of ATAC-seq from T47D breast cancer cells treated with DMSO or BYL719 (1 μM) for 24 hours. The red dots correspond to the accessible sites upon BYL719 treatment. **(B)** Heat map of accessible sites gained upon BYL719 treatment, shown in a horizontal window of ±3 kb from the peak center. (**C**) The top enriched motifs of the accessible sites upon BYL719 treatment: ERE ($P = 1 \times 10^{-11}$); FOXA1 ($P = 1 \times 10–^{205}$); and PBX1, homeobox ($P = 1 \times 10–^{144}$). (**D**) Examples of ChIP-seq ER- and FOXA1-binding regions and ATAC-seq open chromatin regions in T47D breast cancer cells and tumor samples from breast cancer patients treated with BYL719 (in reads per million). The patient samples were collected before the commencement of treatment with BYL719 (“Pre”) and after ~14 days of treatment (“On”). The latter samples were collected between 2 and 6 hours after administration of the drug. **(E)** The enriched motifs of the accessible sites gained upon BYL719 treatment. Patient 1 enriched motifs: Esrra, nuclear receptor class ($P = 1 \times 10–^{15}$);

FOXA1 ($P = 1 \times 10^{-22}$); and PBX1, homeobox ($P = 1 \times 10^{-24}$). Patient 2 enriched motifs: ERE ($P = 1 \times 10^{-6}$); forkhead class ($P = 1 \times 10^{-7}$), and PBX1, homeobox ($P = 1 \times 10^{-5}$).

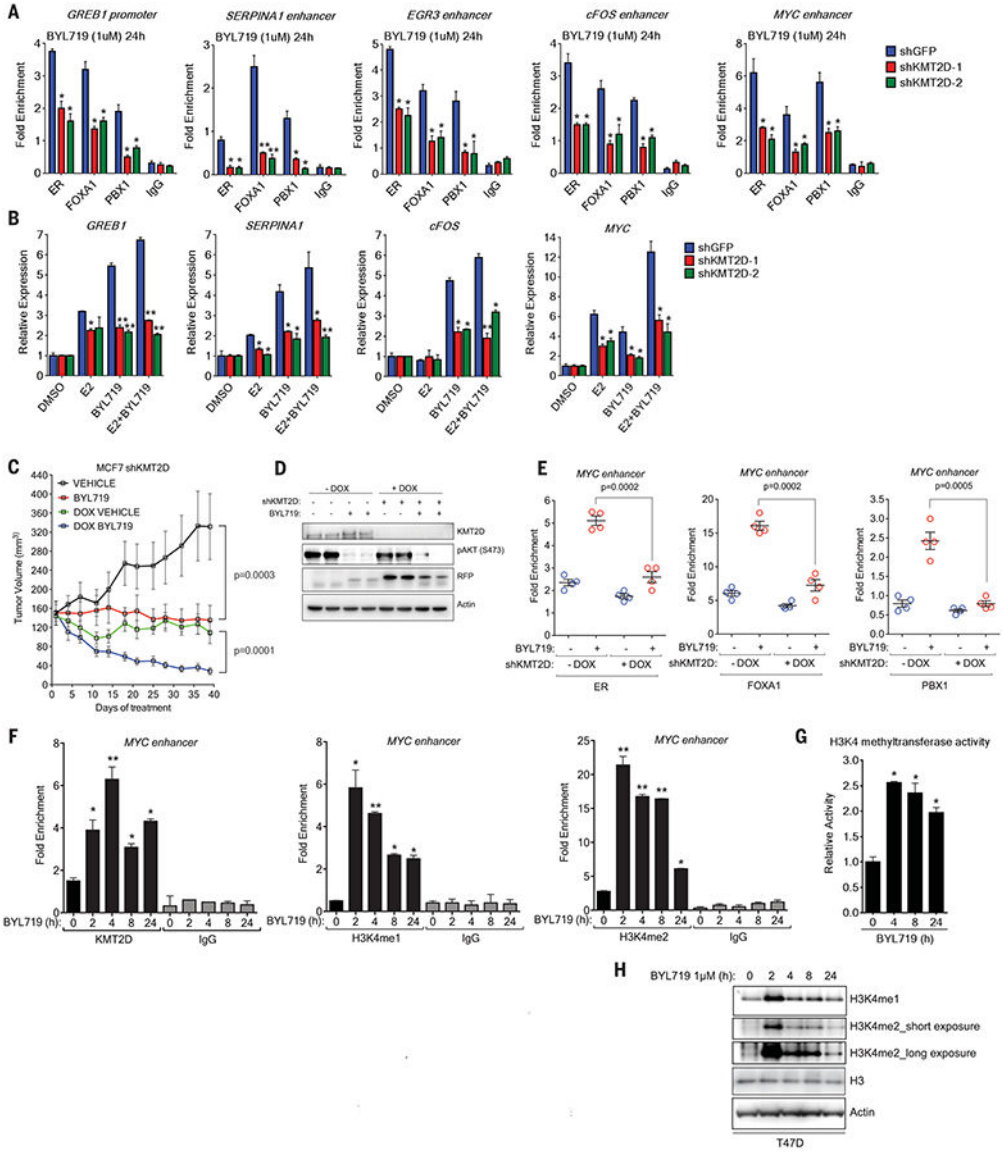

Fig. 3. Activation of ER-dependent transcription by PI3Kα pathway inhibition is regulated by the histone H3K4 methyltransferase KMT2D

(**A**) ChIP-qPCR assay of ER, F0XA1, PBX1, and control IgG binding at the candidate target genes, after KMT2D was knocked down by two distinct shRNAs, in T47D breast cancer cells upon treatment with BYL719 (1 μM) for 24 hours. GFP, green fluorescent protein. Error bars, SD ($n = 3$). *$P < 0.05$, **$P < 0.01$; Student's t test. (**B**) RT-qPCR in estrogen-depleted T47D cells for 3 days, followed by treatment with DMSO, E2 (100 nM), BYL719 (1 μM), or E2 plus BYL719 for 24 hours. Values are the average of 3 replicates. *$P < 0.05$, **$P < 0.01$; Student's t test. (**C**) MCF7 shKMT2D doxycycline-inducible in vivo xenograft treated daily with vehicle or BYL719 (25 mg/kg) ($n = 10$ per group). The indicated P values were calculated using Student's t test. Error bars, ±SEM. (**D**) Western blot analysis of lysates of tumors collected at the end of the experiment. RFP, red fluorescent protein. (**E**) Tissue ChIP-qPCR analysis of ER, F0XA1, and PBX1 binding at the candidate target genes of tumors collected at the end of the experiment, 4 hours after the last BYL719 dose. P values

were calculated using Student's *t* test. Error bars, ±SEM. (**F**) ChlP-qPCR for KMT2D, H3K4mel, H3K4me2, and IgG control in T47D breast cancer cells treated with BYL719 (1 μM) for 2,4,8,12, and 24 hours. Error bars, SD ($n = 3$). *$P < 0.05$, **$P < 0.01$; Student's *t* test. (**G**) H3K4 methyltransferase activity of T47D nuclear extracts after the cells were treated with BYL719 (1 μM) for 4,8, and 24 hours.The substrate was a synthetic H3 peptide, and the activity was measured using a H3K4 methyltransferase kit. Error bars, SD ($n = 3$). *$P < 0.05$; Student's *t* test. (**H**) Immunoblot analysis of H3K4mel, H3K4me2, H3, and actin in T47D cells after treatment with BYL719 (1 μM) for 2, 4, 8, and 24 hours.

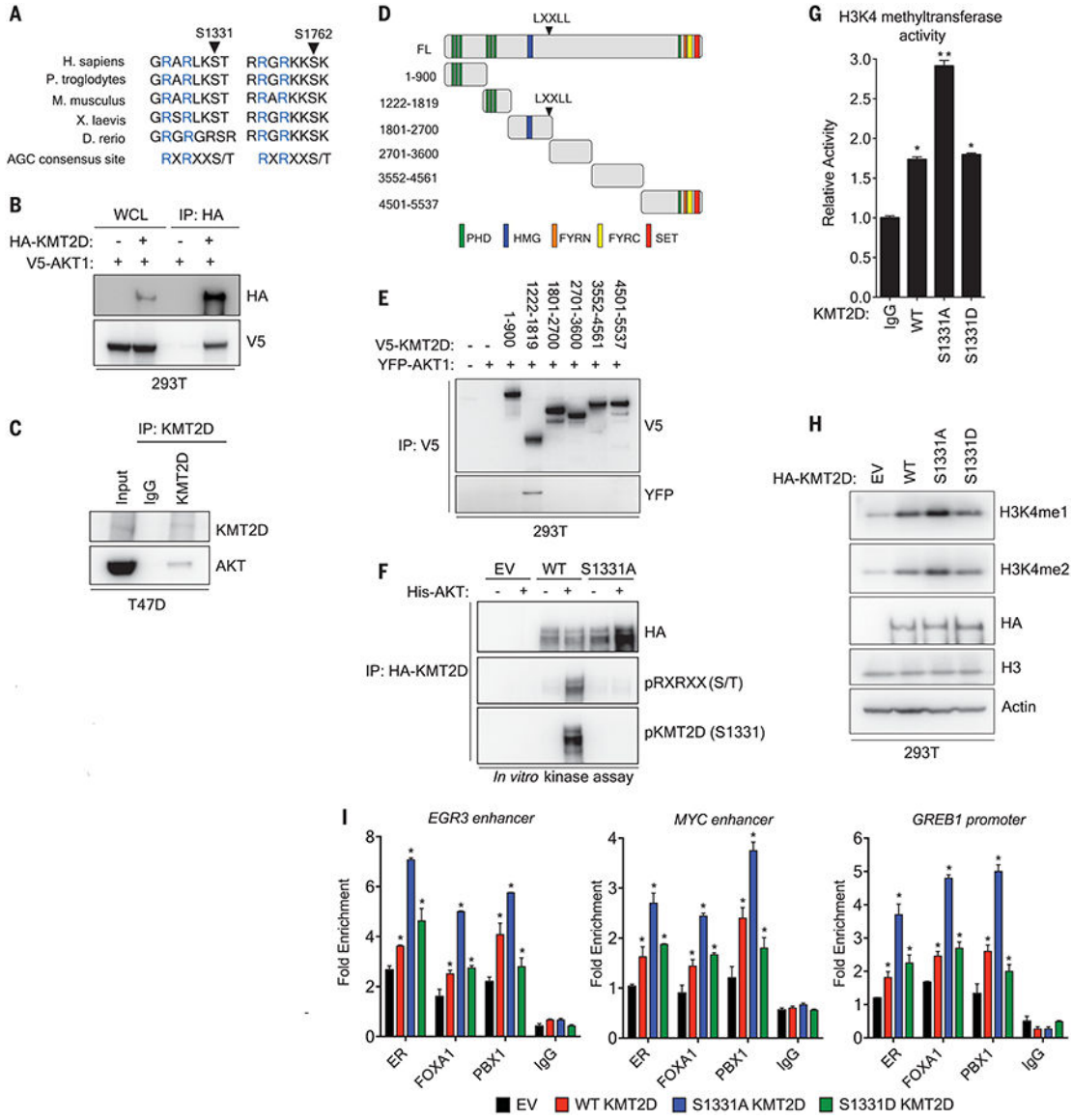

Fig. 4. AKT1 interacts with and phosphorylates KMT2D, attenuating its activity. (A) In silico analysis of AGC phosphorylation motifs RXRXX(S/T) 'R, arginine; X, any amino acid; (S/T), phosphorylatable serine or threonine'. Rl and R3 are highlighted in blue, and phosphorylatable S is indicated by the black triangle. Alignment was performed with CustalW2, using KMT2D protein sequences from chimpanzee (*Pan troglodytes*), mouse (*Mus musculus*), frog (*Xenopus laevis*), and zebrafish (*Danio rerio*). G, glycine; A, alanine; L, leucine; K, lysine. (**B**) Co-immunoprecipitation (IP) assay in 293Tcells transfected with the indicated plasmids and probed with HA and V5 antibodies. WCL, whole cell lysate. **(C)** Coimmunoprecipitation of endogenous KMT2D and AKT in T47D breast cancer cells and immunoblotted with KMT2D and AKT antibodies. (**D**) Schematic representation of different truncated fragments of KMT2D used for coimmunoprecipitation assays (FL, full length). Also shown are the key domains of the KMT2D protein: PHD, plant homeodomain; HMG, high mobility group; FYRN, FY-rich N-terminal; FYRC, FY-rich C-terminal; SET,

Su(var)3-9, enhancer-of-zeste, trithorax domain; LXXLL, nuclear receptor recognition motif. **(E)** Coimmunoprecipitation assays in 293T cells transfected with yellow fluorescent protein (YFP)-AKTl and each of the indicated V5-tagged KMT2D fragments. **(F)** In vitro kinase assay using recombinant His-AKTand wild-type (WT) KMT2D or S1331A KMT2D immunoprecipitated from 293Tcells as a substrate, treated with MK2206 (2 (μM) for 1 hour. EV, empty vector. **(G)** H3K4 methyltransferase activity of IgG control, WT, S1331A, and S1331D KMT2D immunoprecipitated from 293Tcells. The substrate was a synthetic H3 substrate, and the activity was measured using a H3K4 methyltransferase kit. D, aspartic acid. Error bars, SD ($n = 3$). *$P < 0.05$, **$P < 0.01$; Student's t test. **(H)** Immunoblot analysis of the indicated histone methylation marks in 293Tcells transfected with control, WT, S1331A, and S1331D KMT2D vectors. **(I)** ChlP-qPCR of ER, F0XA1, PBX1, and IgG control binding in ER target genes in T47D cells expressing WT, S1331A, and S1331D KMT2D. Error bars, SD ($n = 3$). *$P < 0.05$; Student's t test.